Aalborg Universitet

An active damper for stabilizing power electronics-based AC systems

Wang, Xiongfei; Blaabjerg, Frede; Liserre, Marco; Chen, Zhe; He, J.; LI, Y.

An Active Damper for Stabilizing Power Electronics-Based AC Systems

X. Wang, F. Blaabjerg, M. Liserre, and Z. Chen
Department of Energy Technology, Aalborg University
Pontoppidanstraede 101, 9220 Aalborg, Denmark
Email: {xwa, fbl, mli, zch}@et.aau.dk

J. He and Y. Li
Department of Electrical and Computer Engineering
University of Alberta, Edmonton, Canada
Email: {hjinwei, yunwei.li}@ualberta.ca

Abstract—**The mutual interactions between the parallel grid-connected converters coupled through the grid impedance tend to result in a number of stability and power quality challenges. To address them, this paper proposes an active damper concept based on a low-power, high-bandwidth power converter. The basic idea behind this proposal is to dynamically adjust the grid impedance seen from the point of common coupling of the grid-connected converters, such that the potential instabilities and resonance propagation can be effectively mitigated. Simulation and laboratory tests on three parallel grid-connected converters are carried out. The results validate the stabilizing performance of the active damper.**

I. INTRODUCTION

Over the last years, the power electronics converters are gaining a wide acceptance as an efficient grid interface for connecting renewable energy systems and at the load side as electric drives [1], [2]. The mutual interactions between the controllers of the parallel grid-connected converters coupled via the grid impedance, such as the wind turbines converters in wind farms [3], the Photovoltaic (PV) inverters in PV power plants [4], and the locomotive converters in the electric railway networks [5], will inevitably arise, which may result in small-signal oscillations. Furthermore, due to the popular use of *LCL*-filters, additional resonances may occur in the parallel grid-connected converters and vary with the different number of converters. This fact in turn reduces the allowed bandwidth of the converters, and also in some cases tends to introduce undamped resonances [6]-[8].

There is, consequently, an urgent need to develop effective measures to address the aforementioned challenges. In [9], the impedance-based stability analysis method, originating from the Middlebrook's Extra Element Theorem [10], provides a powerful tool to gain the insight of the converter interactions. It has been shown that a non-negative real part of the input admittance of a grid-connected converter is usually required for the damping of oscillations [11]. Hence, to dampen out the additional resonances brought by the parallel-connected *LCL*-filters, the Resistive-Active Power Filter (R-APF) method is adopted for the parallel grid-connected PV inverters in [12],

where the inverters are controlled to behave as resistive loads at the non-fundamental frequencies. However, in this case, a high-bandwidth current controller is needed in order to cover the changes of resonant frequencies, which may be difficult to realize for the high power converter applications. Also, the performance of the R-APF approach is affected by the grid-side inductances in the *LCL*-filters [13]. As opposite to the use of the virtual resistance loop, a filter-based method is reported in [3], where a wideband notch filter covering the resonance frequencies is inserted into the current controller, and thus the resonances in a wind power plant can be damped. The main drawback of this method is the design of the wideband notch filter, which is highly dependent on the system conditions and the stabilizing performance tends to be degraded under the system parameters variations.

In this work, instead of reshaping the input impedances of grid-connected converters by using the different control loops, an active damper based on a low-power, high-frequency, and high-bandwidth power electronic converter is proposed. This active damper is connected to the Point of Common Coupling (PCC) of the grid converters, and aims to dynamically adjust the grid impedance via the variable resistances at the resonance frequencies which appear. Hence, the instabilities and resonances resulting from the interactions in the parallel grid-connected converters can effectively be mitigated.

This paper first presents a small-signal stability analysis of a power electronics-based AC system in Section II, including two parallel active rectifiers with the *LCL*-filters. The mutual interactions between the rectifiers and the influence of the grid impedance variations are evaluated by the Nyquist stability criterion. Then, in light of the analysis results, the operation principle of the proposed active damper concept is discussed in Section III including the basic configuration and the control schemes. This is followed by an assessment on the damping effect of the active damper in the frequency-domain. Finally, in Section IV, to further validate the stabilizing performance of the active damper, simulations and laboratory tests on the two parallel active rectifiers as well as the active damper are performed. The results show that the resonances raised in the system are damped by the active damper.
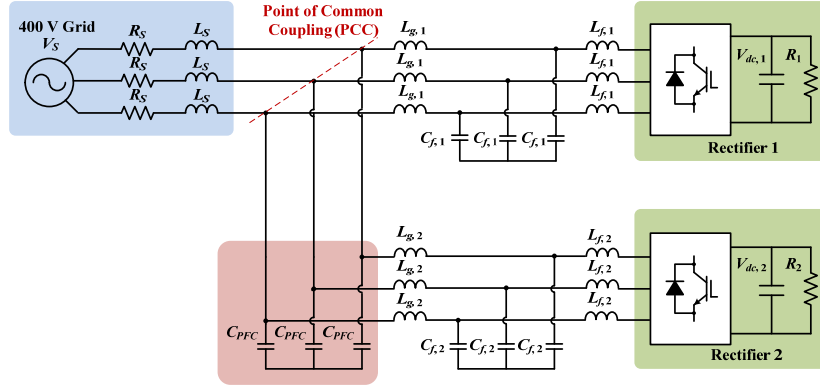
Fig. 1. A three-phase power electronics-based AC system.

II. STABILITY ANALYSIS OF PARALLEL GRID-CONNECTED CONVERTERS WITH *LCL*-FILTERS

Fig. 1 illustrates a three-phase power electronics-based AC system, where two active rectifiers are connected in parallel, respectively, to the Point of Common Coupling (PCC), and a Power Factor Correction (PFC) capacitor C_{PFC} is installed at the PCC. In such a system, the presence of shunt-connected capacitors in the *LCL*-filters and the PFC capacitor may lead to resonances at the different frequencies than the case of single active rectifier [5]. These additional resonances in turn reduce the stability margins of the control loops of the rectifiers, and even result in unstable oscillations. To clarify the nature of such resonances and small-signal oscillations, the impedance-based stability analysis that is based on the terminal behavioral models of the converters is carried out [9], [14].

A. Modeling of Parallel Grid-Connected Converters

Fig. 2 represents the simplified circuit for the *i*-th (*i*=1, 2) active rectifier. The converter is represented by the modulated voltage source $V_{M,i}$, and the grid-side current is controlled for a better stability of the control system [15]. Thus, the frequency behavior of the *LCL*-filter at the PCC can be expressed by the following admittances

$$Y_{M,i} = \left. \frac{I_{g,i}}{V_{M,i}} \right|_{V_{PCC}=0} = \frac{Z_{Cf,i}}{Z_{Cf,i}Z_{Lf,i} + Z_{Lg,i}Z_{Lf,i} + Z_{Cf,i}Z_{Lg,i}} \quad (1)$$

$$Y_{o,i} = \left. \frac{-I_{g,i}}{V_{PCC}} \right|_{V_{M,i}=0} = \frac{1}{Z_{Cf,i}Z_{Lf,i} + Z_{Lg,i}Z_{Lf,i} + Z_{Cf,i}Z_{Lg,i}} \quad (2)$$

where $Z_{Lf,i}$, $Z_{Cf,i}$ and $Z_{Lg,i}$ are the impedances for the inductor $L_{f,i}$, the capacitor $C_{f,i}$, and the inductor $L_{g,i}$, respectively.

Fig. 3 shows the block diagram of the current control loop for the *i*-th active rectifier, which is applied in the synchronous *dq*-frame. Since the dynamics of the outer DC voltage control loop, the reactive power control loop, and the phase locked-loop are much slower than the current control loop, the effects of these control loops are neglected for the sake of simplicity. Consequently, the terminal behavior of the *i*-th rectifier can be represented by a Norton equivalent circuit, as shown in Fig. 4,
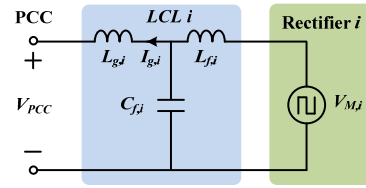
Fig. 2. Simplified circuit for the *i*-th (*i*=1, 2) active rectifier.
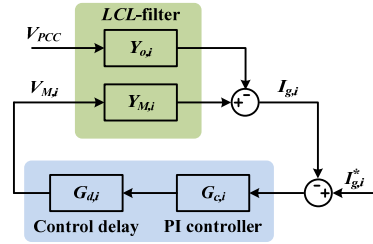
Fig. 3. Block diagram of the current control loop for the *i*-th active rectifier.
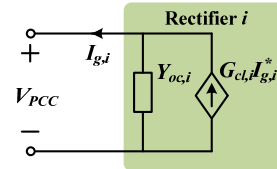
Fig. 4. The Norton equivalent circuit for the *i*-th active rectifier with the grid-side current control loop closed.

which are derived as follows

$$I_{g,i} = G_{cl,i}I_{g,i}^* - Y_{oc,i}V_{PCC} \quad (3)$$

$$G_{cl,i} = \frac{T_{c,i}}{1+T_{c,i}} \quad (4)$$

$$Y_{oc,i} = \frac{Y_{o,i}}{1+T_{c,i}} \quad (5)$$

where $I_{g,i}^*$ is the current reference of the *i*-th converter, $G_{cl,i}$ is the closed-loop gain of the current control loop, and $Y_{oc,i}$ is

the closed-loop input admittance. $T_{c,i}$ is the open-loop gain of the current control loop, which is derived as

$$T_{c,i} = G_{c,i} G_{d,i} Y_{M,i} \qquad (6)$$

where $G_{c,i}$ is the Proportional-Integral (PI) current controller, and $G_{d,i}$ is the approximated 1.5 sampling period ($T_{s,i}$) delay in the digital control, which are expressed as follows

$$G_{c,i} = K_{pc,i} + \frac{K_{ic,i}}{s} \qquad (7)$$

$$G_{d,i} = e^{-1.5 T_{s,i} s} \approx \frac{1 - 0.75 T_{s,i} s + \left(1.5 T_{s,i} s / 12\right)^2}{1 + 0.75 T_{s,i} s + \left(1.5 T_{s,i} s / 12\right)^2} \qquad (8)$$

Substituting the active rectifiers shown in Fig. 1 by the Norton equivalent circuits, the closed-loop model of the power electronics-based system can be obtained, as shown in Fig. 5. Y_C is the admittance of the PFC capacitor C_{PFC}, Z_S is the grid impedance including L_S and R_S. It is clear that there are three closed-loop gains for characterizing the responses of the grid-side current in the i-th active rectifier, which are expressed as

$$I_{g,i} = \frac{G_{cl,i}}{1 + T_{m,i}} I_{g,i}^* - \frac{T_{m,i}}{1 + T_{m,i}} I_{g,j}^* - \frac{T_{m,i}}{1 + T_{m,i}} \frac{V_S}{Z_S} \qquad (9)$$

where the term 'j' denotes the other active rectifier ($i \neq j$). $T_{m,i}$ is the derived minor-loop gain used for the impedance-based stability analysis [14], which is given by

$$T_{m,i} = \frac{Y_{oc,i}}{Y_{t,i}}, \quad Y_{t,i} = \frac{1}{Z_S} + Y_C + Y_{oc,j} \qquad (10)$$

where $Y_{t,i}$ is the total sum of the closed-loop input admittance of the other j-th rectifier and the grid admittance, as well as the admittance of the PFC capacitor.

B. Impedance-based Stability Analysis

To confirm the correctness of the derived minor-loop gain, the mutual interactions between the two active rectifiers and the effect of grid impedance variations are assessed in both the frequency- and time-domain. Table I summarizes the electrical constants for the power electronics-based AC system shown in Fig. 1. The main controller parameters of the active rectifiers are listed in Table II.

Fig. 6 depicts the frequency response of the open-loop gain of the current control loop $T_{c,i}$ in the i-th active rectifier. It is seen that a stable closed-loop terminal behavior of the rectifier is obtained at the PCC. Then, considering the effect of grid impedance, single active rectifier with the PFC capacitor at the PCC is evaluated. Fig. 7 compares the Nyquist plots for the minor-loop gains $T_{m,i}$, which is derived with the different grid inductances. It is shown that the current control loop becomes unstable when the grid inductance L_S is equal to 0.6 mH.

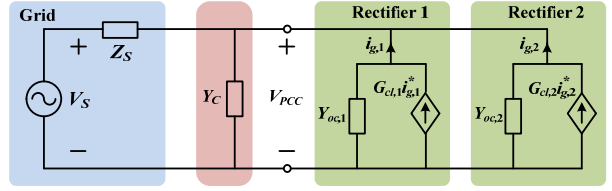Fig. 8 shows the Nyquist plots of the minor-loop gains by

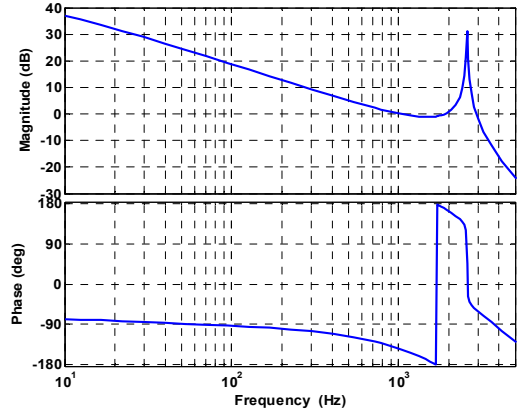Fig. 5. Closed-loop model of the power electronics-based AC system.

Fig. 6. Frequency response of the open-loop gain of the current control loop in the i-th rectifier.
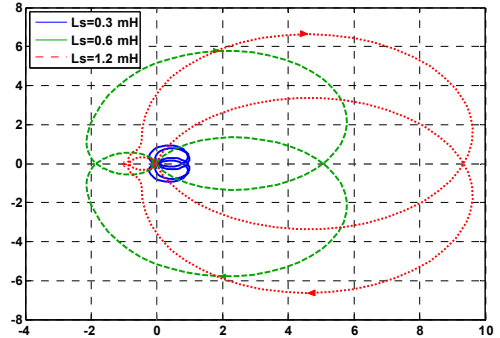
Fig. 7. Nyquist plots of the minor-loop gains derived with the different grid inductance in the case of single active rectifier.

taking the input admittance of the other paralleled rectifier into account. Since in the case of L_S equal to 0.6 mH the current control loop is already unstable for single active rectifier, it is not involved in Fig. 8. It is interesting to notice that the current control loop is unstable in the case that L_S is equal to 1.2 mH, rather than marginally stable as shown in Fig. 6. Furthermore, in order to identify the resonance frequencies in this case, Fig. 9 depicts the frequency responses of $Y_{oc,i}$ and $Y_{t,i}$. It is seen that two admittances intersect at 1740 Hz with a negative phase margin, which indicates that a resonance will arise around this frequency.

To further confirm the above frequency-domain analysis, the time-domain simulations of the parallel active rectifiers are performed with SIMULINK and PLECS. Fig. 10 shows the simulated currents in the case of single active rectifier with the different grid inductances, from which a good match with the Nyquist plots shown in Fig. 7 can be observed. Fig. 11 shows
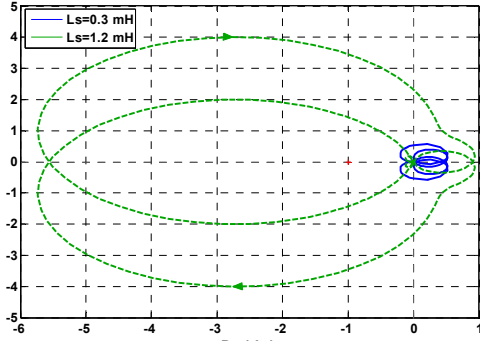
Fig. 8. Nyquist plots of the minor-loop gains with the effect of the input admittance of the other parallel active rectifier.
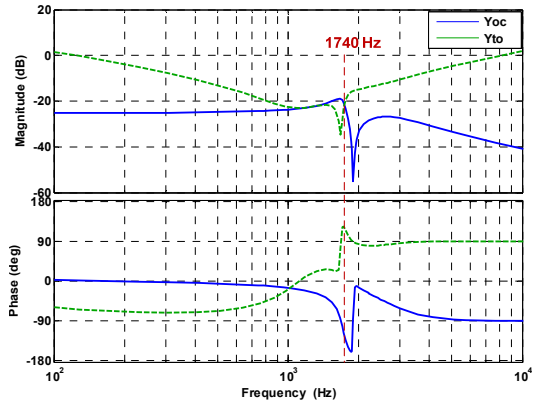
Fig. 9. Frequency responses of $Y_{oc,i}$ and $Y_{t,i}$ in the unstable case (L_S = 1.2 mH) for identifying the resonance point.
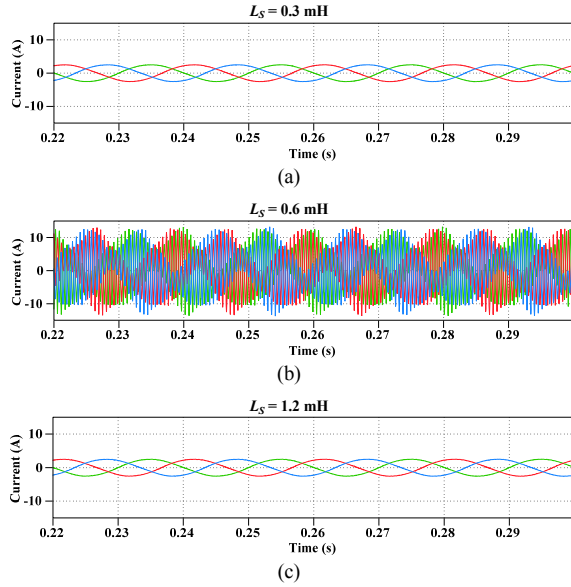
Fig. 10. Simulated current waveforms in the case of single active rectifier. (a) L_S = 0.3 mH. (b) L_S = 0.6 mH. (c) L_S = 1.2 mH.

the simulated currents of the parallel active rectifiers. It is seen that the resonances arise when L_S is equal to 1.2 mH. Fig. 12 gives the current harmonic spectra in the unstable case, which validates the resonance frequency analysis in Fig. 9.

(a)

(b)

Fig. 11. Simulated currents of the parallel active rectifiers. (a) L_S = 0.3 mH. (b) L_S = 1.2 mH.

Fig. 12. Current harmonic spectra in the unstable case (L_S = 1.2 mH).

Fig. 13. Basic configuration of the proposed active damper.

III. Proposed Active Damper

From (10), it is known that the grid impedance Z_S results in a coupling between the parallel active rectifiers. As in the case of an ideally stiff power grid, there are no interactions between the controllers of rectifiers. Thus, the idea behind the proposed active damper is to introduce a variable damping resistance via the power converter into the grid impedance profile in order to effectively dampen out the system resonances.

A. Operation Principle

Fig. 13 shows a basic configuration of the proposed active damper, which consists of a three-phase, two-level voltage source converter and a resonance damping controller. Since there is no additional energy storage element at the DC-link, only the active power responsible for keeping a constant DC voltage is consumed by the active damper.

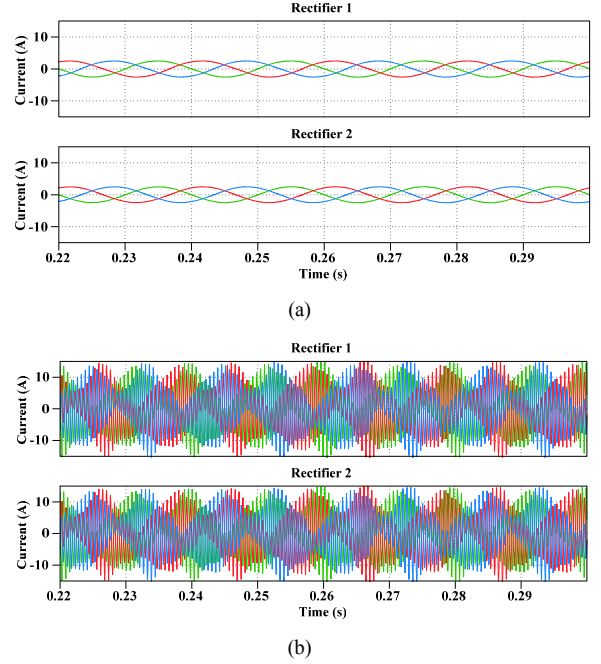Furthermore, the active damper is only responsible for the damping of resonances caused by the controller interactions in the parallel grid-connected converters, which is different from the conventional active power filters for steady-state harmonic current compensation. The power rating of the active damper is thus lower than active power filters, which allows operating with a high switching frequency. As a consequence, a high-bandwidth controller which covers a wide variety of resonance frequencies can be achieved.

Fig. 14 illustrates two types of control block diagrams for realizing such an active damper function. The first option is based on a conventional Resistive-Active Power Filter (R-APF) method [16], as shown in Fig. 14 (a). However, instead of emulating resistance at all the non-fundamental frequencies as usual, only the resonant components of the PCC voltage are detected and divided by a virtual conductance in this scheme.

Fig. 14 (b) shows the block diagram of the second control scheme, where multiple frequency-adaptive resonant voltage controllers are employed to achieve the direct resonant voltage compensation. The outputs of the resonant voltage controllers are passed directly to the duty cycle of the active damper, thus a fast response of resonance damping can be obtained. Also, the design of the inner current controller is easier compared to the R-APF method, which is merely to ensure a constant DC voltage of the active damper.

It is worthy to mention that the resonance detection plays

(a)

(b)

Fig. 14. Two control block diagrams for realizing the proposed active damper function. (a) R-APF method. (b) Direct voltage compensation scheme.

an important role in the above two control schemes. A couple of research works have been reported on the identifying the resonance frequencies [17], [18]. To reduce the computation time, the resonant controller with a wide band can be used to extract or compensate the resonant voltage components.

B. Stabilizing Effect of Active Damper

To see the stabilizing effect of the proposed active damper, the minor-loop gain is evaluated with the damping resistance provided by the active damper. In light of the analysis result in Fig. 9, the wide band-pass filter with the center frequency at 1740 Hz and a bandwidth of 100 Hz is used to synthesize the damping resistance. As a consequence, the active damper can be represented in the frequency-domain as follow

$$R_{d,e} = \frac{\omega_c s}{s^2 + \omega_c s + \omega_0^2} R_{d,ref} \qquad (11)$$

where $R_{d,e}$ and $R_{d,ref}$ are the effective and referenced damping resistance provided by the active damper, respectively. ω_0 and ω_c denote the center frequency and the bandwidth of the band-pass filter, respectively.

Fig. 15 depicts the Nyquist plots for the minor-loop gains with the different damping resistances of the active damper. It is shown that for the unstable case of parallel active rectifiers ($L_S = 1.2$ mH), the system is stabilized with the decrease of the damping resistance. Also, the frequency responses of Y_{oc} and Y_{to} are shown in Fig. 16, from which it can be seen that the intersection points between the two admittances disappear when $R_{d,ref}$ is equal to 5 Ω.

IV. SIMULATION AND EXPERIMENTAL RESULTS

To further validate the performance of the proposed active damper, the time-domain simulations and laboratory tests are performed on three grid-connected converters. Two converters are used to build the parallel active rectifiers shown in Fig.6, and the last converter is controlled as the active damper. Table III gives the main parameters of the active damper.

A. Simulation Results

Corresponding to the simulated currents shown in Fig. 11 and Fig.12, the stabilizing performances of the active damper are evaluated in the cases of single active rectifier and parallel active rectifiers, respectively. The direct voltage compensation scheme is tested.

Fig. 17 shows the simulated PCC voltage and current for the unstable case of single active rectifier (L_S=0.6 mH) before and after applying the proposed active damper. In this case, the active damper is enabled at the time instant of 0.24 s. It is obvious that the resonance resulting from the grid impedance variation is damped by the active damper.

Fig. 18 shows the simulated currents for the unstable case of parallel active rectifiers (L_S=1.2 mH) after using the active damper. Compared to Fig. 11, it can be seen that the mutual interactions between the two active rectifiers are stabilized by the active damper. The change of the PCC voltage when the active damper is applied at the instant of 0.24 s is shown in Fig.9. An effective resonance damping on the PCC voltage can be observed.

In this case, the output current of the active damper and the associated harmonic spectra are depicted in Fig. 20. It can be
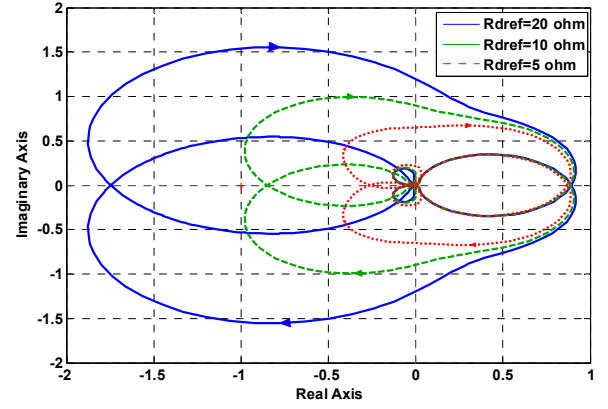

Fig. 15. Nyquist plots of the minor-loop gains with the different damping resistances of the active damper.
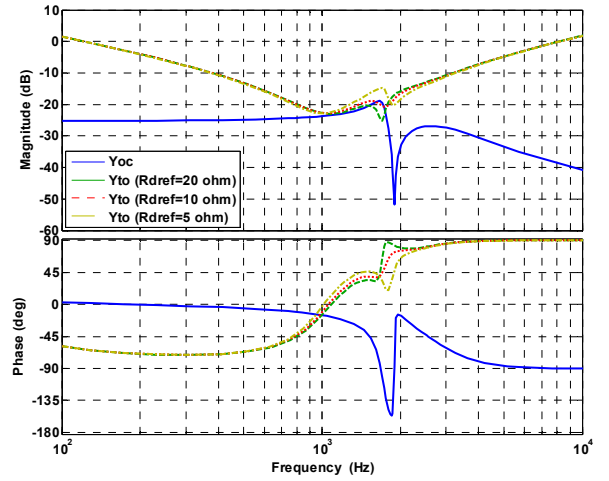

Fig. 16. Frequency responses of the input admittance of one rectifier and the total sum of the other admittances considering the effect of the active damper.
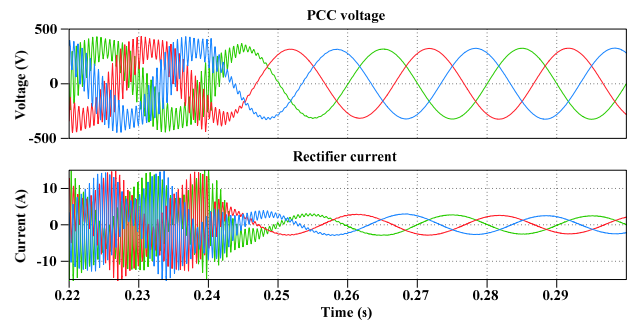

Fig. 17. Simulated PCC voltage and current for the unstable case of single active rectifier (L_S=0.6 mH) before and after applying the active damper.

seen that the fundamental frequency current is low due to the absence of the energy storage element in the DC side, while the resonant current components are relatively large compared to the fundamental frequency current. This fact implies that the active damper has to absorb a certain amount of resonance currents for stabilizing the parallel active rectifiers.
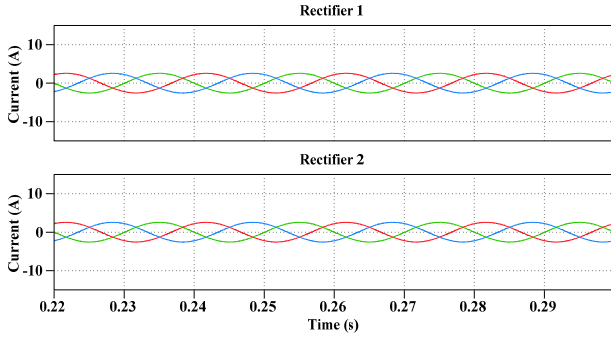
TABLE III. MAIN PARAMERRES OF ACTIVE DAMPER

Parameters		Values
Filter inductance	$L_{f,D}$	3 mH
DC capacitor	$C_{dc,D}$	660 μF
Switching frequency	f_{sw}	20 kHz
Sampling period	T_S	5×10^{-5} s
DC voltage	$V_{dc,D}$	700 V
PR current controller	K_{p_i}	30
	K_{r_i}	600
DC voltage controller	$K_{p\_dc,D}$	0.05
	$K_{i\_dc,D}$	0.5
Resonant controllers	K_{r_v}	2
	ω_r	3500π rad/s

Fig. 18. Simulated currents for the unstable case of parallel active rectifiers (L_S=1.2 mH) after using the active damper.
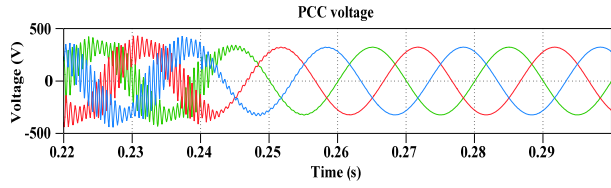

Fig. 19. The change of the PCC voltage when the active damper is applied at the time instant 0.24 s.
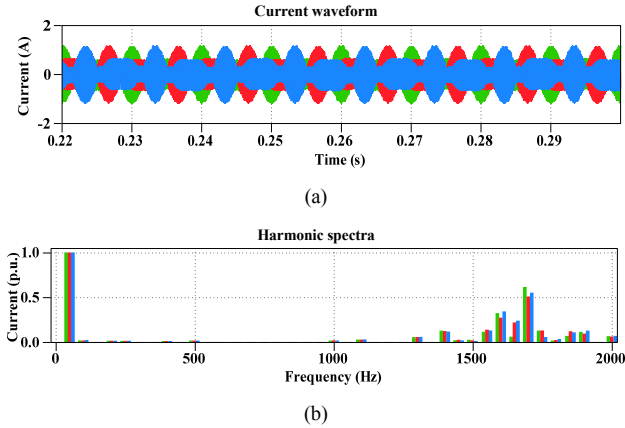

(a)

(b)

Fig. 20. Simulated current of the active damper and the associated harmonic spectra. (a) Current waveform. (b) Harmonic spectra.

B. Experimental Results

In the laboratory test setup, three parallel grid-connected Danfoss converters are used to build the power electronics-based system shown in Fig. 1 as well as the proposed active damper. The control systems are implemented in the DS1006 dSPACE system, where the DS5101 digital waveform output board is used to generate the switching pulses.

Fig. 21 depicts the tested PCC voltage waveform without applying the proposed active damper, and Fig. 22 gives the harmonic spectra of the measured PCC voltage waveform. It is clearly shown that a low-order harmonic resonance (650 Hz) is raised in this case. Also, the tested output currents of the two active rectifiers are shown in Fig. 23. It can be observed that the same low-order harmonic resonance components arise in the output currents.
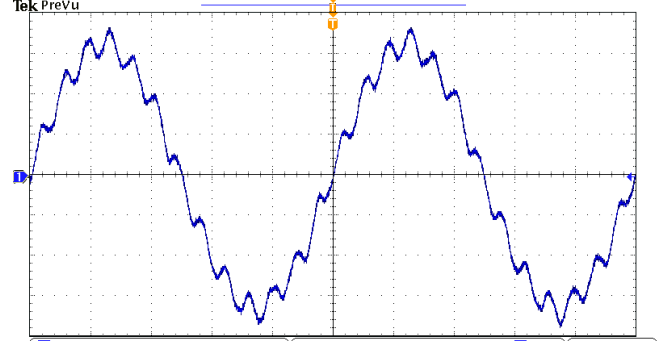

Fig. 21. Measured PCC voltage waveform without applying the active damper (100 V/div, 4 ms/div).
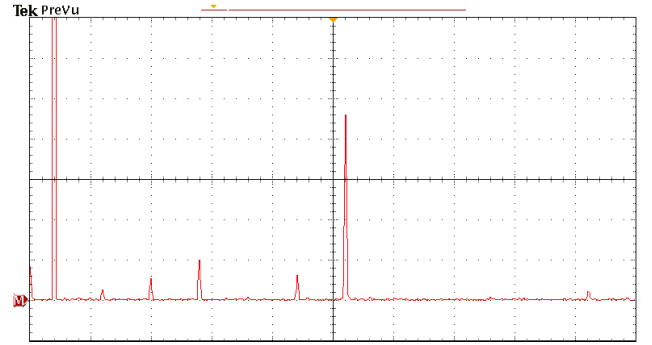

Fig. 22. Harmonic spectra of the measured voltage without applying the active damper (2 V_{RMS}/div, 125 Hz/div).
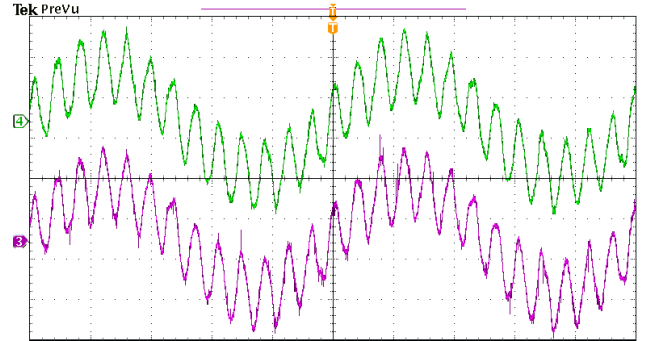

Fig. 23. Measured output current waveforms of the parallel active rectifiers without applying the active damper. (2 A/div, 4 ms/div).

This fact is due to the use of the twelfth harmonic resonant current controller in the synchronous frame for the harmonic current compensation. In the case of single active rectifier, this harmonic resonant current controller works well. However, when the two active rectifiers are connecting in parallel, the measured current waveforms indicate that the phase margins of the current control loops are reduced because of the mutual interactions between the two rectifiers.

Fig. 24 shows the measured PCC voltage waveform after applying the active damper. It is evident that the harmonic resonance is effectively damped by the active damper. Fig. 25 shows the measured output currents of the parallel active rectifiers. It can be seen that the low-order harmonic currents
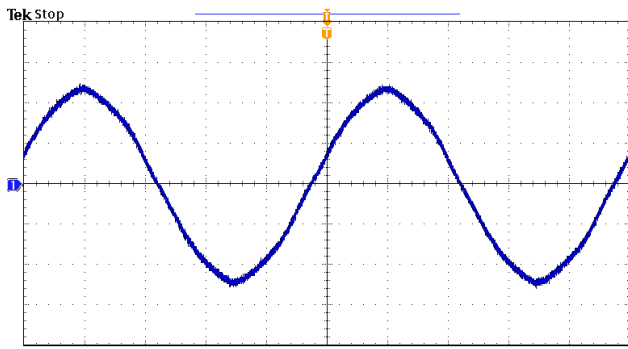
Fig. 24. Measured PCC voltage waveform after applying the active damper (100 V/div, 4 ms/div)
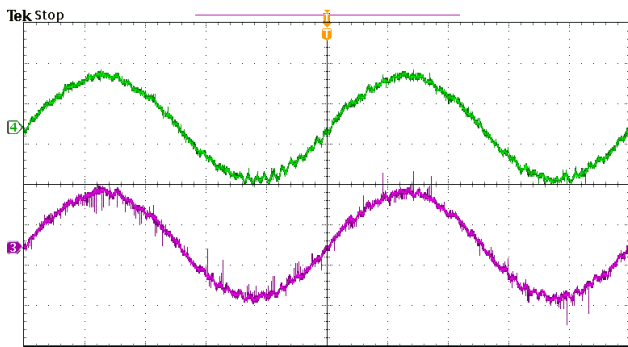

Fig. 25. Measured output current waveforms of the parallel active rectifiers after applying the active damper. (2 A/div, 4 ms/div)

are compensated by using the harmonic resonant controllers. It validates that the proposed active damper can help to stabilize the mutual interactions between the current control loops of the parallel grid-connected converters.

V. CONCLUSIONS

This paper has discussed the resonance propagation in the multiple parallel grid-connected converters. An active damper for stabilizing the power electronics-based AC systems has been proposed. Although a number of active stabilization methods have been reported in previous work, most of them are embedded in the control systems of the converters. As a consequence, the performances of those approaches are either limited by the characteristics of converters or sensitive to the system conditions, which may cause additional resonances. In contrast, the proposed active damper aims to provide a versatile device that can be plug-and-play for the different applications. Furthermore, in comparison to the conventional active power filters, the active damper only takes effect for the resonance damping, which allows a low-power, high control bandwidth design. Two control options for realizing the active damper function have been discussed. Notice that the direct voltage compensation scheme can perform the same function as the resistive-active power filter method by choosing the gains of the resonant controllers based on the desired damping resistances. Simulations and experimental results have been

shown and have confirmed the stabilizing performance of the proposed active damper.

REFERENCES

[1] F. Blaabjerg, Z. Chen, and S. B. Kjaer, "Power electronics as efficient interface in dispersed power generation systems," *IEEE Trans. Power Electron.*, vol. 19, pp. 1184-1194, Sep., 2004.

[2] J. Rocabert, A. Luna, F. Blaabjerg, and P. Rodriguez, "Control of power converters in AC microgrids," *IEEE Trans. Power Electron.*, vol. 27, pp. 4734-4749, Nov., 2012.

[3] P. Brogan, "The stability of multiple, high power, active front end voltage sourced converters when connected to wind farm collector system," in *Proc. EPE* 2010, pp. 1-6.

[4] J. Agorreta, M. Borrega, J. Lopez, and L. Marroyo, "Modeling and control of *N*-paralleled grid-connected inverters with *LCL* filter coupled due to grid impedance in PV plants," *IEEE Trans. Power Electron.*, vol. 26, pp. 770-785, Mar., 2011.

[5] E. Mollerstedt and B. Bernhardsson, "Out of control because of harmonics–An analysis of the harmonic response of an inverter locomotive," *IEEE Control Sys. Mag.,* vol. 20, pp. 70-81, Aug., 2000.

[6] X. Lu, M. Liserre, K. Sun, F. Blaabjerg, R. Teodorescu, and L. Huang, "Resonance propagation of parallel-operated DC-AC converters with LCL filters," in *Proc. IEEE APEC* 2012, pp. 877-884.

[7] R. Turner, S. Walton, and R. Duke, "Stability and bandwidth implications of digitally controlled grid-connected parallel inverters," *IEEE Trans. Ind. Electron.*, vol. 57, pp. 3685-3694, Nov., 2010.

[8] F. Wang, J. L. Duarte, M. A. M. Hendrix, and P. F. Ribeiro, "Modeling and analysis of grid harmonic distortion impat of aggeragated DG inverters," *IEEE Trans. Power Electron.*, vol. 26, pp. 786-797, Mar., 2011.

[9] J. Sun, "Small-signal methods for AC distributed power systems–a review," *IEEE Trans. Power Electron.*, vol. 24, pp. 2545-2554, Nov., 2009.

[10] R. D. Middlebrook, V. Vorperian, and L. Lindal, "The *N* extra element theorem," *IEEE Trans. Circuits Syst. I: Fundam. Theory Appl.*, vol. 45, pp. 919-935, Sep., 1998.

[11] L. Harnefors, M. Bongiorno, and S. Lundberg, "Input-admittance calculation and shaping for controlled voltage-source converters," *IEEE Trans. Ind. Electron.*, vol. 54, pp. 3323-3334, Dec., 2007.

[12] J. He, Y. W. Li, D. Bosnjak, and B. Harris, "Investigation and active damping of multiple resonances in a parallel-inverter-based microgrid," *IEEE Trans. Power Electron.*, vol. 28, pp. 234-246, Jan., 2013.

[13] X. Wang, F. Blaabjerg, and Z. Chen, "Synthesis of variable harmonic impedance in inverter-interfaced distributed generation unit for harmonic damping througout a distribution network," *IEEE Trans. Ind. Appl.*, vol. 48, pp. 1407-1417, Jul./Aug., 2012.

[14] J. Sun, "Impedance-based stability criterion for grid-connected covnerters," *IEEE Trans. Power Electron.*, vol. 26, pp. 3075-3078, Nov., 2011.

[15] J. Yin, S. Duan, and B. Liu, "Stability analysis of grid-connected inverter with LCL filter adopting a digital single-loop controller with inherent damping characteristic" *IEEE Trans. Ind. Inform.*, Early Access Articles.

[16] H. Akagi, H. Fujita, and K. Wada, "A shunt active filter based on votlage detection for harmonic termination of a radial power distribution line," *IEEE Trans. Ind. Appl.*, vol. 35, pp. 638-645, May/Jun., 1999.

[17] L. Asiminoaei, R. Teodorescu, F. Blaabjerg, and U. Borup, "A digital controlled PV-inverter with grid impedance estimation for ENS detection," *IEEE Trans. Power Electron.*, vol. 20, pp. 1480-1490, Nov., 2005.

[18] X. Zhou, J. Fan, and A. Q. Huang, "High-frequency resonance mitigation for plug-in hybrid electric vehicles' integration with a wide range of grid conditions," *IEEE Trans. Power Electron.*, vol. 27, pp. 4459-4471, Nov., 2012.